ACS Photonics

Article

Cite This: ACS Photonics 2017, 4, 2813-2820

pubs.acs.org/journal/apchd5

Light Soaking Phenomena in Organic–Inorganic Mixed Halide Perovskite Single Crystals

Hye Ryung Byun,[†,‡] Dae Young Park,[†,‡] Hye Min Oh,[†] Gon Namkoong,[*,§] and Mun Seok Jeong[*,†,‡]

[†]Department of Energy Science, Sungkyunkwan University, Suwon, 16419, Republic of Korea

[‡]Center for Integrated Nanostructure Physics, Institute for Basic Science (IBS), Suwon, 16419, Republic of Korea

[§]Department of Electrical and Computer Engineering, Old Dominion University, Applied Research Center, 12050 Jefferson Avenue, Newport News, Virginia 23606, United States

Supporting Information

ABSTRACT: Recently, organic–inorganic mixed halide perovskite ($MAPbX_3$; MA = $CH_3NH_3^+$, X = Cl^-, Br^-, or I^-) single crystals with low defect densities have been highlighted as candidate materials for high-efficiency photovoltaics and optoelectronics. Here we report the optical and structural investigations of mixed halide perovskite ($MAPbBr_{3-x}I_x$) single crystals. Mixed halide perovskite single crystals showed strong light soaking phenomena with light illumination conditions that were correlated to the trapping and detrapping events from defect sites. By systematic investigation with optical analysis, we found that the pseudocubic phase of mixed halide perovskites generates light soaking phenomena. These results indicate that photoinduced changes are related to the existence of multiple phases or halide migrations.

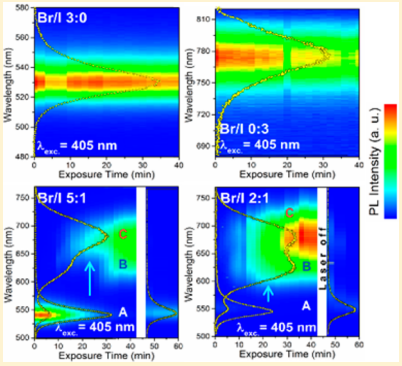

KEYWORDS: *light soaking effect, perovskite single crystal, photoluminescence, time-resolved photoluminescence*

Organic–inorganic mixed halide perovskites ($MAPbX_3$; MA = $CH_3NH_3^+$, X = Cl^-, Br^-, or I^-) have been highlighted as potential photovoltaics[1−6] and optoelectronics[7−9] due to their outstanding optoelectronic properties sich as high absorption coefficients,[2] tunable band gaps, and long carrier diffusion lengths.[10,11] Perovskite thin films can be prepared by a simple spin-coating method. However, solution-processed perovskite thin films inherently contain high densities of defects including defective grain boundaries, surface/point defects, and others.[12−14] Recently our groups reported that the grain boundaries are composed of high oxygen content but scarcity of Pb, Cl, and I, serving as nonradiative recombination centers.[15] Among the related research to reduce the defect density, the perovskite single crystal has been predominantly studied.[16−18] To date, several studies of perovskite single-crystal-based devices have been reported including a thick $MAPbI_3$ single-crystal solar cell with ∼100% internal quantum efficiency[16] and tunable response spectra of photodetectors from mixed halide perovskite single crystals.[18]

Currently, there are numerous studies reporting light soaking effects of thin film halide perovskite ($MAPbBr_3$ or $MAPbBr_{3-x}I_x$).[19−21] Until now, underlying mechanisms of light soaking effects of perovskite thin films include (i) charge trapping and detrapping from defect sites,[19] (ii) ion migration,[20] and (iii) disorder.[21] The light soaking effect is a drastic change of optical properties under illumination and is usually observed in hybrid perovskite materials. It should be solved to achieve long-term operational stabilities in hybrid perovskite optoelectronic devices. However, it is expected that perovskite single crystals will have much lower defect densities compared to thin film perovskite films. Therefore, it is expected that the light soaking effect might be different from that of thin film perovskite. Nonetheless, the light soaking effect of perovskite single crystals has not been studied yet.

In this study, we report the optical and structural properties of mixed halide perovskite ($MAPbBr_{3-x}I_x$) single crystals to investigate their underlying mechanisms of the light soaking effect. Mixed halide perovskite single crystals were synthesized with different mixing ratios. To confirm the crystallinity of perovskite single crystals, we performed UV–vis absorption and X-ray diffraction (XRD). The XRD peaks of perovskite single crystals of mixed Br/I were located between the cubic phase ($MAPbBr_3$) and the tetragonal phase ($MAPbI_3$) at room temperature. In addition, we measured persistent photoluminescence (PL) and time-resolved PL (TRPL) spectroscopies with increasing laser irradiation time. We also performed XRD measurements on mixed halide perovskite single crystals after white-light illumination. Particularly, we found that the light soaking effect was strongly dependent upon the compositions of perovskite single crystals in which the cubic phase ($MAPbBr_3$) and the tetragonal phase ($MAPbI_3$) showed weak light soaking effects. In contrast, mixed halide perovskite

Received: July 20, 2017
Published: October 6, 2017

DOI: 10.1021/acsphotonics.7b00797
ACS Photonics 2017, 4, 2813−2820

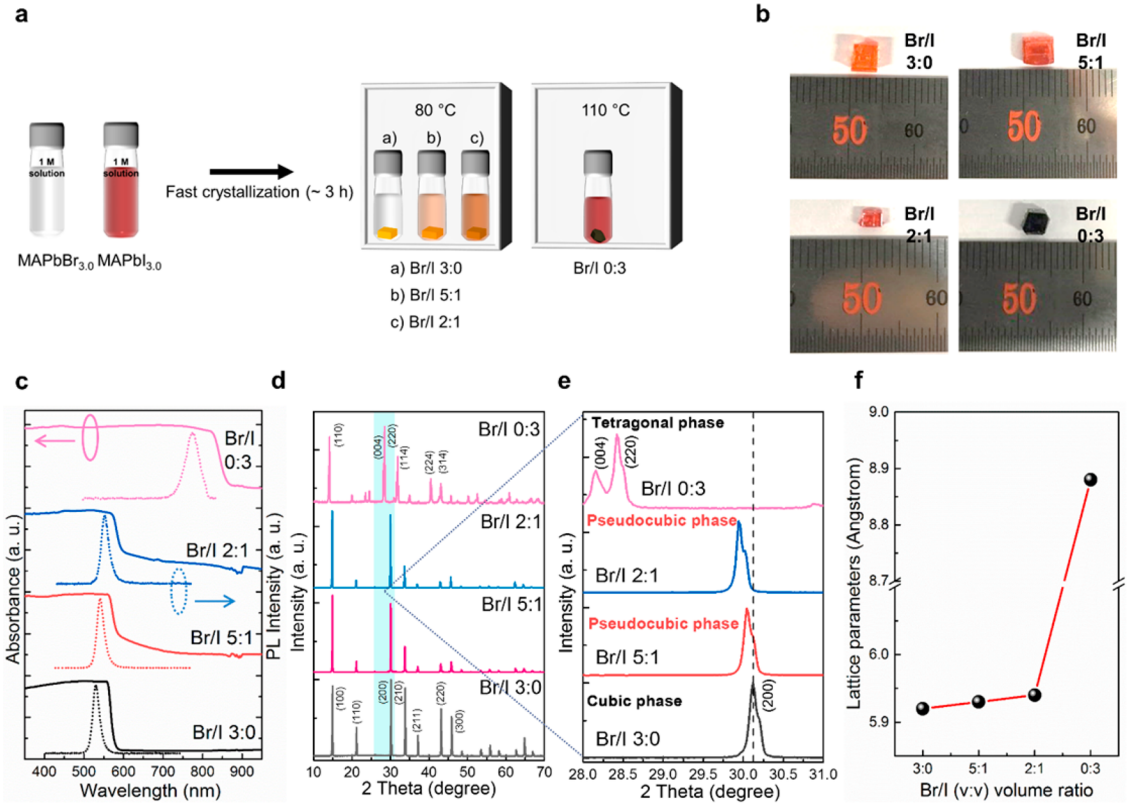

Figure 1. Single-crystal growth process. (a) Schematic of the single crystals fabricated by the inverse temperature crystallization method with the crystallization vial dipped in an oven. The solutions are heated in an oven and kept at a high temperature (80 °C for Br/I 3:0, Br/I 5:1, and Br/I 2:1 and 110 °C for Br/I 0:3) to initiate crystallization. (b) Mixed halide perovskite single crystal growth at different mixing ratios: Br/I 3:0, Br/I 5:1 (top) and Br/I 2:1, Br/I 0:3 (bottom). Steady-state absorption, photoluminescence, and powder X-ray diffraction. (c) UV−vis absorption and PL spectra of $MAPbBr_{3-x}I_x$ perovskite single crystals. (d) XRD patterns of $MAPbBr_{3-x}I_x$ perovskite single crystals. (e) XRD patterns of $MAPbBr_{3-x}I_x$ perovskite single crystals, enlarged in the region of the cubic (200) and tetragonal (004) and (220) peaks (2θ = 28.0−31.0°). (f) Lattice parameters of $MAPbBr_{3-x}I_x$ perovskite single crystals as a function of I composition.

single crystals showed strong light soaking effects with light illumination conditions that were correlated to the trapping and detrapping events from defect sites.

RESULTS AND DISCUSSION

The perovskite single crystals were synthesized by modified inverse temperature crystallization (ITC).[16,22−25] The detailed perovskite single crystal preparation procedure is described in Figure 1a. Degrees of coordination in the perovskite single crystals could possibly be tailored by combining different solvents and precursor solutions.[26−28] In previous reports, $MAPbBr_3$ and $MAPbI_3$ single crystals were grown as high-quality, fast-crystallized, shape-controlled single crystals.[17] $MAPbBr_3$ crystallized more pertinently from *N*,*N*-dimethylformamide (DMF), while $MAPbI_3$ crystallized better from γ-butyrolactone (GBL).[22] Consequently, the syntheses of $MAPbBr_{3.0}$ and $MAPbI_{3.0}$ were performed with DMF- and GBL-based ITC methods, respectively. The filtrate (1.5 mL) was placed in a vial, and the vial was kept in an oven at 80 and 110 °C for Br- and I-based mixed halide perovskite single crystals, respectively ($MAPbBr_{3-x}I_x$ perovskite single crystal mixing ratio: $MAPbBr_{3.0}$:$MAPBI_{3.0}$ = 5:1 (v/v), i.e., $MAPbBr_{2.5}I_{0.5}$; $MAPbBr_{3.0}$:$MAPBI_{3.0}$ = 2:1 (v/v), i.e., $MAPbBr_{2.0}I_{1.0}$), as illustrated in Figure 1a. (See Methods section for details.) Figure 1b shows a snapshot of the perovskite single crystals; the size distribution of the samples was about 3 mm. We further verified the absence of GBs in the single crystals via scanning electron microscopy (SEM), and the energy-dispersive X-ray spectroscopy (EDS) data show the different mixing ratios of Br and I (see Supporting Information (SI), Figure S1).

From the UV−vis absorption and PL measurements, a sharp band edge and narrow bandwidth were observed (Figure 1c). The band gaps extracted from Tauc plots showed values of 2.17, 2.12, 2.06, and 1.46 eV for Br/I 3:0, Br/I 5:1, Br/I 2:1, and Br/I 0:3, respectively (see SI, Figure S2).[29] The PL peak position of Br/I 3:0, Br/I 5:1, Br/I 2:1, and Br/I 0:3 single crystals was located at 530 (2.34 eV), 540 (2.30 eV), 554 (2.24 eV), and 773 nm (1.60 eV), respectively.

To confirm the crystallinity of the $MAPbBr_{3-x}I_x$ single crystals, powder XRD measurements were performed at room temperature. XRD patterns of the single crystals (Figure 1d) demonstrate the pure perovskite phase of both Br/I 3:0 and Br/I 0:3. Br/I 3:0 and Br/I 0:3 had cubic and tetragonal perovskite phases at room temperature, respectively, which are in agreement with previous single crystals grown using the antisolvent vapor-assisted crystallization (AVC) method.[22] The XRD patterns were monitored in the 2θ range from 28.0° to 31.0° for $MAPbBr_{3-x}I_x$ with increasing I ions, as shown in Figure 1e. In Br/I 0:3 ($MAPbI_{3.0}$), two peaks were located at 28.11° and 28.36°, which indicate the (004) and (220) planes for the tetragonal *I*4/*mcm* phase.[30] According to previous reports, the tetragonal *I*4/*mcm* phase is obtained from the cubic $Pm\bar{3}m$ phase in the classic $MAPbX_3$ perovskite structure by the slight rotation of PbX_6 octahedra along the ⟨001⟩ axis on the

DOI: 10.1021/acsphotonics.7b00797
ACS Photonics 2017, 4, 2813−2820

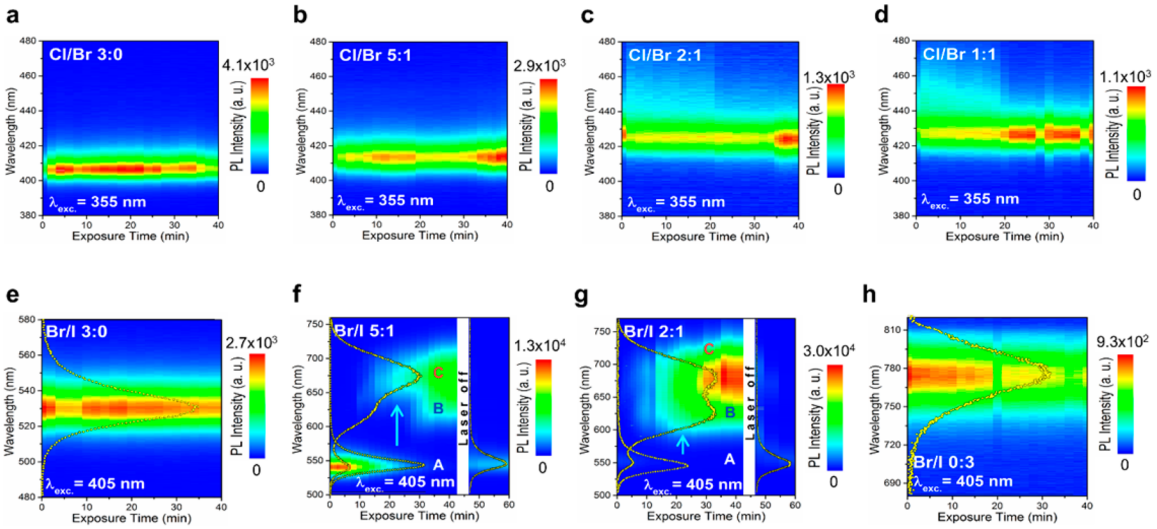

Figure 2. Contour plots of PL spectra of Cl/Br and Br/I (v/v = 3:0, 5:1, 2:1, 1:1, 0:3) single crystals as a function of laser irradiation time. (a) Cl/Br 3:0, (b) Cl/Br 5:1, (c) Cl/Br 2:1, (d) CI/Br 1:1, (e) Br/I 3:0, (f) Br/I 5:1, (g) Br/I 2:1, and (h) Br/I 0:3. (f and g) In the pseudocubic phase perovskite single crystals, the A, B, and C peaks in the PL spectra were reproduced by assuming three peaks with Gaussian functions. The yellow lines of (e) and (h) are the spectra at laser irradiation time 0 min. Similarly, the yellow lines of (f) are spectra at 0 and 30 min next to the solid arrow and the yellow lines of (g) are spectra at 0 and 6 min next to the solid arrow.

(00*l*) plane while retaining their corner-sharing connectivity; that is, the tetragonal phase can be designated by a pseudocubic lattice.[31] Although previous reports categorized a pseudocubic phase for the tetragonal phase (in the case of the Br/I 0:3), Br/I 0:3 ($MAPbI_3$) referred to here had a pure phase, as did Br/I 3:0 ($MAPbBr_3$). In addition, the mixed halide perovskite single crystals (Br/I 5:1 and Br/I 2:1) denominated here had a pseudocubic phase at room temperature.

To examine the optical properties of mixed halide perovskite single crystals as a function of laser irradiation time, PL measurements were performed at room temperature. Solid-state lasers with wavelengths of 355 and 405 nm were used as excitation sources, and a spectrometer equipped with a grating (150 grooves/500 nm blaze) was utilized for the measurement. During laser irradiation, the PL spectra of the $MAPbCl_{3-x}Br_x$ single crystals maintained band-edge peaks. This finding indicates that the Cl- and Br-perovskite solution mixing ratio has an effect on the emission wavelength of chloride−bromide lead perovskites, as observed in Figure 2a−d. Figure 2e−h show the contour plots of persistent PL spectra of Br- and I-mixed halide perovskite crystals excited by a 405 nm laser. With increasing laser irradiation time, the PL spectra of pure phase perovskite (see Figure 2e and h) maintained a band-edge peak. Further, in the Gaussian fit data (see SI, Figures S3 and S4), the integrated PL intensity, PL peak energy, and full width at half-maximum (fwhm) rarely changed during the laser irradiation time, as observed in Figure S4a, b, g, and h. However, when the laser irradiation time was prolonged, additional satellite peaks appeared at ∼2.0 eV while the original peak gradually disappeared in the pseudocubic phase perovskite (see Figure 2f and g). Interestingly, when the pseudocubic phase perovskites were left for 15 min in the dark, the PL spectra reverted to the initial PL states, indicating that these photoinduced changes are completely reversible. With changing I composition, there was a time difference in the appearance of low-energy peaks of pseudocubic phase perovskite, but they revealed similar behavior with increasing laser irradiation time. As can be seen in Figure 2f and g (see SI, Figure S4c and e), PL intensity from the low-energy peaks became more intense than the original peak. Comparing Figure S4c with Figure S4e, pseudocubic phase perovskite with higher iodine content exhibited higher initial PL intensity at lower energy. This indicates that the Br/I 2:1 single crystal generated more photoinduced change than the Br/I 5:1 single crystal. To confirm that this PL spectral change does not rely on the particular laser source, we performed PL measurements using various (355, 473, and 633 nm) excitation laser sources (see SI, Figure S5). In the PL spectrum measured using a 633 nm excitation laser, however, we did not obtain any signal (not shown). In the PL spectra measured using 355 and 473 nm excitation lasers, pure and pseudocubic phase perovskite single crystals had a similar tendency to the 405 nm excitation laser as a function of the laser irradiation time. This indicates that these PL spectral changes need an excitation source above the band-gap energy. The phenomenon of this additional PL peak at low energy (∼2.0 eV) was recently reported for bromide−iodide lead perovskite films ($MAPb(Br_{1-x}I_x)_3$) and was attributed to the existence of multiple phases.[32,35] Similarly, the Br/I mixed single crystal may have multiple phases because $MAPbBr_3$ is a cubic phase and $MAPbI_3$ is a tetragonal phase. Therefore, it shows additional PL peak due to the light soaking effect after long time laser irradiation. On the other hand, the Cl/Br mixed single crystal has only a cubic phase at room temperature, so there is no light soaking effect.

We also carried out persistent PL measurements under vacuum to confirm environmental effects (see SI, Figure S6). The additional peak at low energy also appeared under vacuum conditions, indicating that this phenomenon is due to photoinduced changes and not surface adsorbates under ambient conditions.

To investigate the derivation of the observed abnormal behavior of the PL emission peak, TRPL experiments were conducted and the results were analyzed using the charge trapping/detrapping model from defect sites.[33] The trapping and detrapping rates correspond to the number of empty trap states and occupied trap states, respectively. Accordingly, the carrier decay dynamics in terms of charge trapping and detrapping may depend on the density of filled and unfilled

DOI: 10.1021/acsphotonics.7b00797
ACS Photonics 2017, 4, 2813−2820

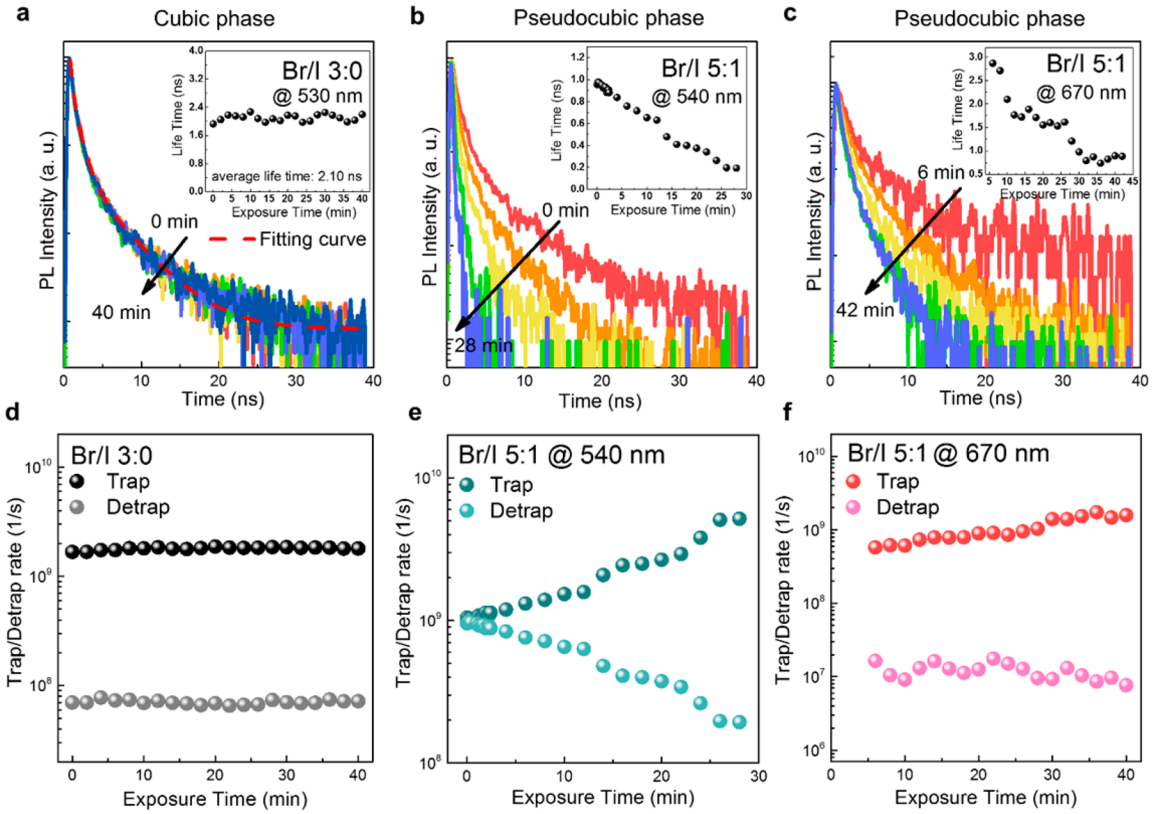

Figure 3. Carrier lifetime measurement. (a, b, and c) PL decay curves monitored as a function of laser irradiation time ((a) pure phase single crystal; (b) and (c) original peak and low-energy peak of pseudocubic phase single crystal, respectively). Insets: PL decay times of the center peak. The PL decay times were obtained by calculation of trapping and detrapping rates through $\tau = (k_{trap} + k_{detrap})^{-1}$. (d, e, and f) Trapping and detrapping rates of perovskite single crystals upon laser irradiation.

trap states and can be described by the following equations:[34−38]

$$\frac{dn(t)}{dt} = -k_{trap}n(t) + k_{detrap}n_{trap}(t) - k_{deep}n(t) \quad (1)$$

$$\frac{dn_{trap}(t)}{dt} = k_{trap}n(t) - k_{detrap}n_{trap}(t) - k_{deep}n_{trap}(t) \quad (2)$$

Here, n, n_{trap}, k_{trap}, k_{detrap}, and k_{deep} are the density of free electrons, the density of electrons in the traps, the trapping rate, the detrapping rate, and the deep-trapping rate, respectively. In our case, deep trap states were not considered because density functional theory (DFT) calculations have proposed that shallow traps are easier to occupy than deep traps.[39] These rate equations can be solved analytically as below:

$$n(t) = \frac{n(0)}{k_{trap} + k_{detrap}}(k_{trap}e^{-(k_{trap}+k_{detrap})t} + k_{detrap}) \quad (3)$$

$$n_{trap}(t) = \frac{n(0)}{k_{trap} + k_{detrap}}(-k_{trap}e^{-(k_{trap}+k_{deptrap})t} + k_{trap}) \quad (4)$$

Thus, a set of equations can be used to fit the carrier decay lifetime to exhibit the trapping and detrapping rates. Figure 3a−c display the PL decay curves at room temperature monitored along the laser irradiation time for the main peak of the cubic phase, the main peak of the pseudocubic phase, and the low-energy peak of the pseudocubic phase perovskite, respectively. The carrier lifetimes calculated from trapping and detrapping rates using $\tau = (k_{trap} + k_{detrap})^{-1}$ are shown in the inset of Figure 3a−c. For laser irradiation time-dependent experiments, decay curves were measured every 2 min, and their trapping and detrapping rates were fitted and plotted in Figure 3d−f. During laser irradiation, the decay behavior of cubic phase perovskite showed nearly constant lifetime, and the average decay time was about 2.10 ns (Figure 3a). The trapping and detrapping rates also showed nearly constant values, as observed in Figure 3d. On the other hand, the decay time of the main peak of the pseudocubic phase perovskite drastically dropped with increasing laser irradiation time (see Figure 3b), while the decay time of the lower energy peak of the pseudocubic phase perovskite decreased until it saturated (see Figure 3c). Interestingly, a substantial rise of trapping rate of the original peak of the pseudocubic phase perovskite was observed at the onset of laser irradiation, while a considerable drop of the detrapping rate was observed, as shown in Figure 3e. Therefore, the continuous increase of trapping rate and decrease of detrapping rate led to an extremely short lifetime, as shown in Figure 3b. Meanwhile, the trapping and detrapping rates of the lower energy peak of the pseudocubic phase perovskite showed a slight increase and decrease, respectively, as illustrated in Figure 3e. In Figure 3f, even though a slight fluctuation in the detrapping rate was observed, it might not have a large influence on the decay time since the detrapping rate is much lower than the trap rate by almost 2 orders. As shown in Figure 2, the lower energy peak position of the pseudocubic phase perovksite fluctuated with laser irradiation time. Consequently, these TRPL results as a function of laser irradiation time show a similar tendency to the PL data.

DOI: 10.1021/acsphotonics.7b00797
ACS Photonics 2017, 4, 2813−2820

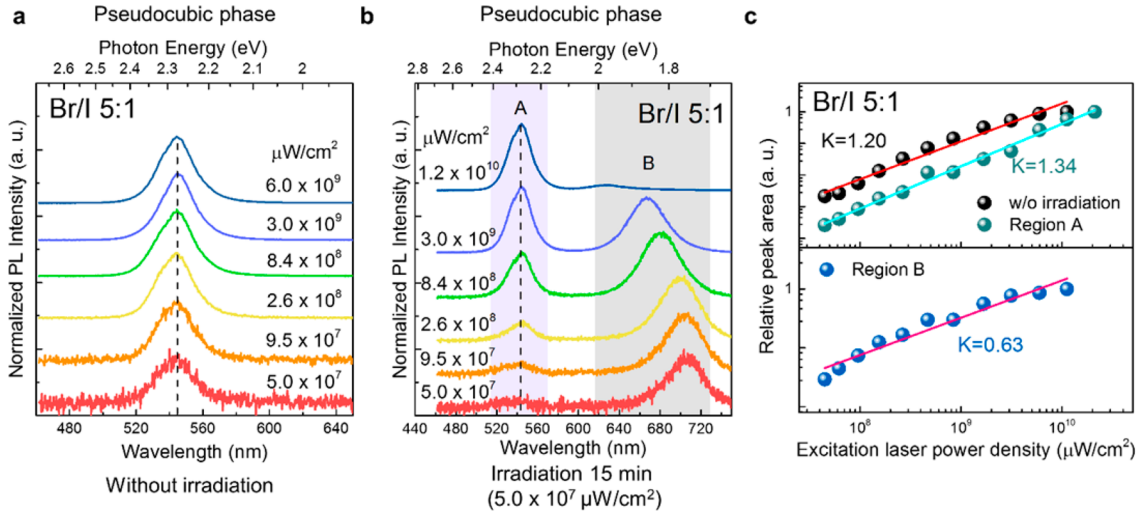

Figure 4. Excitation-power density dependent PL of Br/I 5:1 (pseudocubic phase) single crystals. Power-dependent PL (a) without laser irradiation and (b) after 15 min of laser irradiation. Steady-state PL spectra with excitation density (a) from 5.0×10^7 to 5.2×10^8 μW cm^{-2} and (b) from 5.0×10^7 to 3.0×10^8 μW cm^{-2}. All spectra were measured at RT. (c) Logarithmic plots of the integrated PL intensity versus excitation-power density. Original peaks (without/with laser irradiation, top) and the additional peak of the low-energy peaks (with laser irradiation for 15 min, bottom). The data show a power-law dependence with k = 1.20, 1.34, and 0.63.

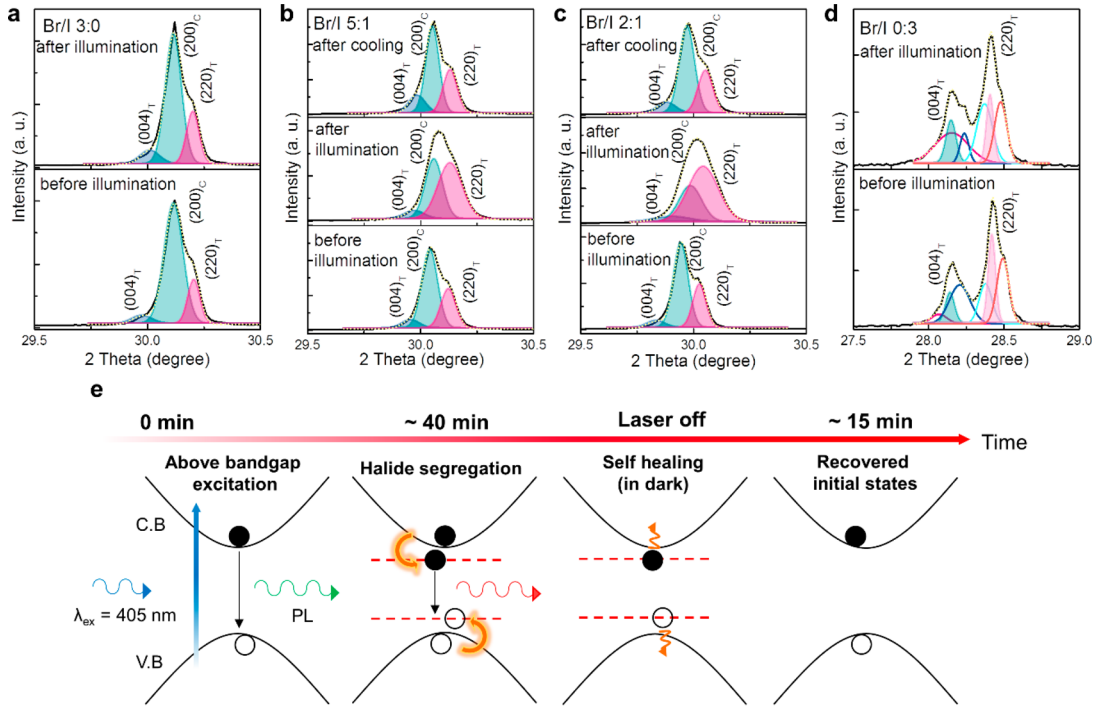

Figure 5. (a)−(d) The (200) XRD pattern of Br/I (v/v = 3:0, 5:1, 2:1, 1:1, 0:3) single crystals before and after white-light illumination for 1 h (white-light illumination at AM 1.5G 100 mW cm^{-2}). The integrated intensity is fit by Gaussian functions. (e) Schematic of the proposed mechanism for abnormal PL behavior of laser irradiation time-dependence based on mixed halide perovskite single crystal band structure evolution by sketching the valence (VB) and conduction (CB) bands for four situations: initial states, photogenerated excitons stabilizing the formation of iodine-rich domains (phase segregation according to increasing laser irradiation time causing the appearance of a lower energy peak), recovery in the dark after laser-off, and recovery of initial states. The red dotted lines represent light-induced metastable self-trap states that relax after laser-off (in the dark) returning to the initial states.

To understand the nature of the lower energy peaks, we performed power-dependent PL measurements as shown in Figure 4. The PL line shapes of the main peak in Figure 4a and b are identical over the entire range of excitation intensities. Figure 4c shows that the PL intensity follows the excitation-power law with an exponent of 1.20 (without irradiation), 1.34 (region A), and 0.63 (region B). These exponent values determined the origin of the PL spectra. Generally, near-band-edge emissions of semiconductors may have various origins such as exciton-like transitions, free-to-bound transitions, band-to-band transitions, and donor−acceptor pair transitions.[39,40] Therefore, under nonresonance conditions in direct-band-gap semiconductors, the luminescence intensity (I_{PL}) follows the power law equation of the excitation density, $I_{PL} \sim I_{ex}^k$, where k

DOI: 10.1021/acsphotonics.7b00797
ACS Photonics 2017, 4, 2813−2820

is the power index with $k < 1$ for free-to-bound and donor−acceptor recombinations, and $1 < k < 2$ for exciton recombination including bound and free excitons.[40] These processes are related to the neutral impurities caused by the photoneutralization of the donor−acceptor pair, which appear in all semiconductor materials. The coefficient $k = 2$ is related to band-to-band recombination. In our power-dependent PL data, the k value corresponds to the previously reported excitation-power dependence of excitons in semiconductors.[41] From these results, we know that the lower energy peaks of pseudocubic phase perovskites are related to defect sites. Further, the peak in region B (see Figure 4b) shifts to higher energy with increasing laser power density. At high excitation-power density, it takes place through a band-filling effect in which photogenerated electrons and holes occupy the higher energy sub-band gaps.[42] This process is expected to contribute to the blue-shifted PL peak position of region B. Another pseudocubic phase perovskite (Br/I 2:1) also has a similar trend of power-dependent PL measurement (see SI, Figure S7).

Because of the appearance of the low-energy peak during laser irradiation and reverting to the initial state in the dark, we propose a photoinduced change related to the phase separation of pseudocubic phase perovskite single crystals. To verify this scenario, we performed XRD measurements on the perovskite single crystals after white-light illumination (see SI, Figure S8a). Figure 5a−d show the $(200)_C$ (cubic phase), $(220)_T$ (tetragonal phase), and $(004)_T$ (tetragonal phase) peaks on a magnified scale. We observed that the pseudocubic phase perovskite single crystals coexist in cubic and tetragonal phases. Jang et al. also showed that the mixed halide perovskite ($MAPbBr_{3-x}I_x$; $x = 0.5-1.0$) nanocrystals have multiple phases.[43] With Gaussian fitting, the XRD diffraction peaks of pure phase perovskites scarcely changed with light irradiation (Figure 5a and d). However, the XRD diffraction peaks of pseudocubic phase perovskites are reversed in intensity ratio of the $(200)_C$ and $(220)_T$ by light irradiation, and the diffraction patterns reverted to the initial state when the pseudocubic phase perovskites were left in the dark state overnight (Figure 5b and c).

Figure S8b shows the PL spectra excited by the 633 nm laser after irradiation with the 473 nm laser for 40 min. The PL spectra of pseudocubic phase perovskite single crystals only appear at the low energy (~1.70 eV); however, PL spectra did not appear without irradiation of the 473 nm laser. These results indicate that there is a metastable state that can be activated with larger energy than the band gap.

To understand the abnormal PL behavior with increasing laser irradiation time, we propose a mechanism based on phase segregation with illumination time in the mixed halide perovskite single crystal, as illustrated in Figure 5e. Under constant laser irradiation, there is an increasing number of photoinduced metastable states (dashed red lines) that accumulate over tens of minutes, causing phase segregation, which results in the lower energy PL peak (phase segregation scheme).[43] However, when the pseudocubic phase perovskite single crystals are rested in the dark (laser off), the dominant photoinduced trap states dissipate and the pseudocubic phase perovskite single crystals revert to nearly 100% of the initial state (self-healing and recovered initial states scheme). This mechanism is similar to the light soaking mechanism of mixed halide perovskite film.[44]

In previous studies, photoinduced halide migration has been reported in $PbBr_2$ and PbI_2.[45] Dawood et al. proposed that the lead metal and iodine are created in a reaction of two excitons at a suitable trapping site, finally leading to the formation of an iodine molecule and an anion vacancy.[46] Verwey has extensively studied the mechanism, which involves the trapping of photogenerated holes to the surface and anion vacancies from the surface to the crystal.[45] The valence band of $MAPb(Br_{1-x}I_x)_3$ contains contributions between the strong Pb s orbital and the halide p orbital antibonding coupling,[47] so we conjecture that the region of iodide-rich domains stabilizes holes. Therefore, the iodide-rich domains could provide a moving enthalpy for halide separation under laser irradiation (phase segregation regime). Further, reversible structural changes in the $PbBr_2$ crystal have been attributed to self-trapped holes and electrons caused by photogeneration.[48] The iodide-rich domains are a stable state under extrinsic change of condition (condition of illumination), but self-trapped states are unstable under intrinsic conditions. Consequently, these processes are activated by laser irradiation, which revert to the initial states in the dark. In addition, to support this mechanism, we performed UV−vis absorption measurement on the perovskite single crystals after white-light illumination and in the dark state (see SI, Figure S9). After the illumination, the band gaps extracted from the Tauc plot in the pure perovskite single crystals are almost unchanged. However, band gaps of the pseudocubic phase perovskite single crystals are changed from 2.12 eV to 1.95 eV (Br/I 5:1) and 2.06 eV to 1.96 eV (Br/I 2:1). These results well matched with the proposed mechanism in Figure 5e.

In contrast, pure phase perovskite single crystals are almost unchanged during laser irradiation. Previous studies have reported that all the perovskite films including pure phase display photoinduced PL enhancement.[21] Generally, this phenomenon is related to the passivation of defects on the perovskite film surface. Zhao et al. show that surface defects work as p-type dopants in perovskite films.[19] Therefore, under illumination, photogenerated charge carriers will be trapped at surface defect sites and make the defects nonactive.[16] Meanwhile, in our research, pure phase perovskite single crystals show no change in the PL features upon laser irradiation, which can be explained by the low defect density of perovskite single crystals.

CONCLUSIONS

We observed the light soaking phenomena in the $MAPbBr_{3-x}I_x$ perovskite single crystals. By systematic investigation with optical analysis, we found that the pseudocubic phase generates light soaking phenomena. On the contrary, there was no change in the PL and TRPL spectra in the pure phase perovskites. For the structural analysis, we performed XRD measurements of $MAPbBr_{3-x}I_x$ perovskite single crystals after white-light illumination. In the case of pseudocubic phase perovskite single crystals, the magnitude of intensity of the cubic and tetragonal phase regions ($(200)_C$ and $(220)_T$) reversed under illumination, which reverted to the initial state after cooling overnight. We suggest that photoinduced changes are fully reversible and relate to the existence of multiple phases or halide migration. These physical changes will be useful for understanding the working mechanisms of perovskite single crystal optoelectronic devices.

DOI: 10.1021/acsphotonics.7b00797
ACS Photonics 2017, 4, 2813−2820

METHODS

Chemicals and Solvents. MABr and MAI were purchased from Dyesol Limited (Australia). Lead bromide (≥98%), DMF (*N*,*N*-dimethylformamide, anhydrous, 99.8%), and GBL (γ-butyrolactone, ≥99%) were purchased from Sigma-Aldrich. Lead iodide (≥99.99%) was purchased from Xi'an Polymer Light Technology Corp. (China). All solvents and salts were used as received without any further purification.

Growth of $CH_3NH_3PbBr_{3-x}I_x$ Single Crystals. $MAPbX_3$ perovskites show inverse temperature solubility behavior in a proper solvent. This phenomenon of mixed halide perovskites allows the design of a new crystallization method for these materials, named inverse temperature crystallization. DMF and GBL were chosen for $MAPbBr_3$ and $MAPbI_3$ ITC, respectively. A solution (1 M) of PbX_2 and MAX was prepared in DMF or GBL for X = Br^- and I^-, respectively. All solutions were prepared at room temperature, ambient condition, and a humidity of 35−40%. The solutions were filtered using a hydrophobic PTFE-D filter with a 0.2 μm pore size. The filtrate (1.5 mL) was placed in a vial, and the vial was kept in an oven at 80 and 110 °C for Br- and I-based mixed perovskites, respectively ($MAPbBr_{3.0}$:$MAPBI_{3.0}$ = 5:1 (v/v), i.e., $MAPbBr_{2.5}I_{0.5}$; $MAPbBr_{3.0}$:$MAPbI_{3.0}$ = 2:1 (v/v), i.e., $MAPbBr_{2.0}I_{1.0}$). The single crystal used for measurement was grown over about 3 h.

Characterization Methods. Field-emission scanning electron microscopy (JSM7000F, JEOL) was performed to examine the surface morphologies of the perovskite single crystals. The elemental compositions of the perovskite single crystals with different mixing ratios were carried out using energy dispersive spectroscopy data in SEM mode. UV−vis absorption spectra were measured using a commercial spectrophotometer (V-670, JASCO) in the range from 300 to 1000 nm. Powder X-ray diffraction was performed on an X-ray diffractometer (Rigaku, SmartLab) with Cu Kα radiation (λ = 1.540 59 Å). $MAPbBr_{3-x}I_x$ single crystals were ground into a powder with a mortar. Bragge−Brentano focusing was operated with a tube at 45 kV and 200 mA. Photoluminescence spectra were obtained using a multifunctional optical microscopy system (NTEGRA SPECTRA, NT-MDT). In this system, a 405 nm (3.06 eV) laser as the excitation source and an excitation power of 0.2 μW were used during the laser irradiation. In-plane spatial resolution of ∼380 nm was indicated by an objective lens (numerical aperture 0.7). For analysis of TRPL, confocal microspectroscopy including a time-correlated single photon counting system was employed (NTEGRA SPECTRA, NT-MDT). The excitation source for the TRPL measurement was a 405 nm pulsed laser with a repetition rate of 20 MHz and a pulse width down to 60 ps. The long time light irradiation measurement was performed under ambient condition with controlled temperature and humidity (24 °C, 42%) in a dark room without UV light. In addition, the samples were stored in the vacuum desiccator after measurement.

ASSOCIATED CONTENT

Supporting Information

The Supporting Information is available free of charge on the ACS Publications website at DOI: 10.1021/acsphotonics.7b00797.

Details of the SEM images of surface, EDS, optical characterization, and XRD results for mixed halide perovskite single crystals (PDF)

AUTHOR INFORMATION

Corresponding Authors

*Phone: +82-31-299-4053. E-mail: gnamkoon@odu.edu.
*E-mail: mjeong@skku.edu.

ORCID

Gon Namkoong: 0000-0002-9795-8981
Mun Seok Jeong: 0000-0002-7019-8089

Notes

The authors declare no competing financial interest.

ACKNOWLEDGMENTS

This work was supported by IBS-R011-D1 of Korea and the National Research Foundation of Korea (NRF) grant funded by the Korean government (MSIP) (2016R1A2B2015581) and Basic Science Research Program through the National Research Foundation of Korea(NRF) funded by Ministry of Education (NRF-2016R1A6A3A11936024).

REFERENCES

(1) Gratzel, M. The light and shade of perovskite solar cells. *Nat. Mater.* **2014**, *13*, 838−842.
(2) Green, M. A.; Ho-Baillie, A.; Snaith, H. J. The emergence of perovskite solar cells. *Nat. Photonics* **2014**, *8*, 506−514.
(3) Kamat, P. V. Organometal Halide Perovskites for Transformative Photovoltaics. *J. Am. Chem. Soc.* **2014**, *136*, 3713−3714.
(4) Hodes, G.; Cahen, D. Perovskite cells roll forward. *Nat. Photonics* **2014**, *8*, 87−88.
(5) Park, N. G. Perovskite solar cells: an emerging photovoltaic technology. *Mater. Today* **2015**, *18*, 65−72.
(6) Liang, J.; Wang, C. X.; Wang, Y. R.; Xu, Z. R.; Lu, Z. P.; Ma, Y.; Zhu, H. F.; Hu, Y.; Xiao, C. C.; Yi, X.; Zhu, G. Y.; Lv, H. L.; Ma, L. B.; Chen, T.; Tie, Z. X.; Jin, Z.; Liu, J. All-inorganic perovskite solar cells. *J. Am. Chem. Soc.* **2016**, *138*, 15829−15832.
(7) Chen, Q.; De Marco, N.; Yang, Y.; Song, T. B.; Chen, C. C.; Zhao, H. X.; Hong, Z. R.; Zhou, H. P.; Yang, Y. Under the spotlight: The organic-inorganic hybrid halide perovskite for optoelectronic applications. *Nano Today* **2015**, *10*, 355−396.
(8) Miyasaka, T. Perovskite Photovoltaics: Rare Functions of Organo Lead Halide in Solar Cells and Optoelectronic Devices. *Chem. Lett.* **2015**, *44*, 720−729.
(9) Liang, J.; Wang, C.; Zhao, P.; Lu, Z.; Ma, Y.; Xu, Z.; Wang, Y.; Zhu, H.; Hu, Y.; Zhu, G.; Ma, L.; Chen, T.; Tie, Z.; Liu, J.; Jin, Z. Solution synthesis and phase control of inorganic perovskites for high-performance optoelectronic devices. *Nanoscale* **2017**, *9*, 11841−11845.
(10) Stranks, S. D.; Eperon, G. E.; Grancini, G.; Menelaou, C.; Alcocer M, J. P.; Leijtens, T.; Herz, L. M.; Petrozza, A.; Snaith, H. J. Electron-Hole Diffusion Lengths Exceeding 1 Micrometer in an Organometal Trihalide Perovskite Absorber. *Science* **2013**, *342*, 341−344.
(11) Younts, R.; Duan, H. S.; Gautam, B.; Saparov, B.; Liu, J.; Mongin, C.; Castellano, F. N.; Mitzi, D. B.; Gundogdu, K. Efficient Generation of Long-Lived Triplet Excitons in 2D Hybrid Perovskite. *Adv. Mater.* **2017**, *9*, 1604278.
(12) Shao, Y. H.; Xiao, Z. G.; Bi, C.; Yuan, Y. B.; Huang, J. S. Origin and elimination of photocurrent hysteresis by fullerene passivation in CH3NH3PbI3 planar heterojunction solar cells. *Nat. Commun.* **2014**, *5*, 5784.
(13) Wang, Q.; Shao, Y. C.; Dong, Q. F.; Xiao, Z. G.; Yuan, Y. B.; Huang, J. S. Large fill-factor bilayer iodine perovskite solar cells fabricated by a low-temperature solution-process. *Energy Environ. Sci.* **2014**, *7*, 2359−2365.
(14) Wu, Z. T.; Luo, Z. Z.; Shen, Y. T.; Zhao, W. W.; Wang, W. H.; Nan, H. Y.; Guo, X. T.; Sun, L. T.; Wang, X. R.; You, Y. M.; Ni, Z. H. Defects as a factor limiting carrier mobility in WSe2: A spectroscopic investigation. *Nano Res.* **2016**, *9*, 3622−3631.

DOI: 10.1021/acsphotonics.7b00797
ACS Photonics 2017, 4, 2813−2820

(15) Namkoong, G.; Jeong, H. J.; Mamun, A.; Byun, H. R.; Demuth, D.; Jeong, M. S. Chemically, spatially, and temporally resolved 2D mapping study for the role of grain interiors and grain boundaries of organic-inorganic lead halide perovskites. *Sol. Energy Mater. Sol. Cells* **2016**, *155*, 134−140.
(16) Dong, Q. F.; Fang, Y. J.; Shao, Y. C.; Mulligan, P.; Qiu, J.; Cao, L.; Huang, J. S. Electron-hole diffusion lengths > 175 mu m in solution-grown CH3NH3PbI3 single crystals. *Science* **2015**, *347*, 967−970.
(17) Saidaminov, M. I.; Abdelhady, A. L.; Murali, B.; Alarousu, E.; Burlakov, V. M.; Peng, W.; Dursun, I.; Wang, L. F.; He, Y.; Maculan, G.; Goriely, A.; Wu, T.; Mohammed, O. F.; Bakr, O. M. High-quality bulk hybrid perovskite single crystals within minutes by inverse temperature crystallization. *Nat. Commun.* **2015**, *6*, 7586.
(18) Fang, Y. J.; Dong, Q. F.; Shao, Y. C.; Yuan, Y. B.; Huang, J. S. Highly narrowband perovskite single-crystal photodetectors enabled by surface-charge recombination. *Nat. Photonics* **2015**, *9*, 679.
(19) Zhao, C.; Chen, B. B.; Qiao, X. F.; Luan, L.; Lu, K.; Hu, B. Revealing Underlying Processes Involved in Light Soaking Effects and Hysteresis Phenomena in Perovskite Solar Cells. *Adv. Energy. Mater.* **2015**, *5*, 150029.
(20) Yoon, S. J.; Draguta, S.; Manser, J. S.; Sharia, O.; Schneider, W. F.; Kuno, M.; Kamat, P. V. Tracking Iodide and Bromide Ion Segregation in Mixed Halide Lead Perovskites during Photoirradiation. *Acs. Energy. Lett.* **2016**, *1*, 290−296.
(21) Gottesman, R.; Gouda, L.; Kalanoor, B. S.; Haltzi, E.; Tirosh, S.; Rosh-Hodesh, E.; Tischler, Y.; Zaban, A.; Quarti, C.; Mosconi, E.; De Angelis, F. Photoinduced Reversible Structural Transformations in Free-Standing CH3NH3PbI3 Perovskite Films. *J. Phys. Chem. Lett.* **2015**, *6*, 2332−2338.
(22) Shi, D.; Adinolfi, V.; Comin, R.; Yuan, M. J.; Alarousu, E.; Buin, A.; Chen, Y.; Hoogland, S.; Rothenberger, A.; Katsiev, K.; Losovyj, Y.; Zhang, X.; Dowben, P. A.; Mohammed, O. F.; sargent, E. H.; Bakr, O. M. Low trap-state density and long carrier diffusion in organolead trihalide perovskite single crystals. *Science* **2015**, *347*, 519−522.
(23) Stoumpos, C. C.; Malliakas, C. D.; Kanatzidis, M. G. Semiconducting Tin and Lead Iodide Perovskites with Organic Cations: Phase Transitions, High Mobilities, and Near-Infrared Photoluminescent Properties. *Inorg. Chem.* **2013**, *52*, 9019−9038.
(24) Dang, Y. Y.; Liu, Y.; Sun, Y. X.; Yuan, D. S.; Liu, X. L.; Lu, W. Q.; Liu, G. F.; Xia, H. B.; Tao, X. T. Bulk crystal growth of hybrid perovskite material CH3NH3PbI3. *CrystEngComm* **2015**, *17*, 665−670.
(25) Baikie, T.; Fang, Y. N.; Kadro, J. M.; Schreyer, M.; Wei, F. X.; Mhaisalkar, S. G.; Graetzel, M.; White, T. J. Synthesis and crystal chemistry of the hybrid perovskite (CH3NH3) PbI3 for solid-state sensitised solar cell applications. *J. Mater. Chem. A* **2013**, *1*, 5628−5641.
(26) Wu, Y. Z.; Islam, A.; Yang, X. D.; Qin, C. J.; Liu, J.; Zhang, K.; Peng, W. Q.; Han, L. Y. Retarding the crystallization of PbI2 for highly reproducible planar-structured perovskite solar cells via sequential deposition. *Energy Environ. Sci.* **2014**, *7*, 2934−2938.
(27) Wakamiya, A.; Endo, M.; Sasamori, T.; Tokitoh, N.; Ogomi, Y.; Hayase, S.; Murata, Y. Reproducible Fabrication of Efficient Perovskite-based Solar Cells: X-ray Crystallographic Studies on the Formation of CH3NH3PbI3 Layers. *Chem. Lett.* **2014**, *43*, 711−713.
(28) Miyamae, H.; Numahata, Y.; Nagata, M. The crystal structure of lead (II) iodide-dimethylsulfoxide (1/2), PbI2 (dmso) 2. *Chem. Lett.* **1980**, *9*, 663−664.
(29) Tauc, J. Optical properties and electronic structure of amorphous Ge and Si. *Mater. Res. Bull.* **1968**, *3*, 37−46.
(30) Kojima, A.; Teshima, K.; Shirai, Y.; Miyasaka, T. Organometal Halide Perovskites as Visible-Light Sensitizers for Photovoltaic Cells. *J. Am. Chem. Soc.* **2009**, *131*, 6050.
(31) Noh, J. H.; Im, S. H.; Heo, J. H.; Mandal, T. N.; Seok, S. I. Chemical Management for Colorful, Efficient, and Stable Inorganic-Organic Hybrid Nanostructured Solar Cells. *Nano Lett.* **2013**, *13*, 1764−1769.
(32) Sadhanala, A.; Deschler, F.; Thomas, T. H.; Dutton, S. E.; Goedel, K. C.; Hanusch, F. C.; Lai, M. L.; steiner, U.; Bein, T.; Docampo, P.; Cahen, D.; Friend, R. H. Preparation of Single-Phase Films of CH3NH3Pb(I1-x,Br-x)(3) with Sharp Optical Band Edges. *J. Phys. Chem. Lett.* **2014**, *5*, 2501−2505.
(33) Hoke, E. T.; Slotcavage, D. J.; Dohner, E. R.; Bowring, A. R.; Karunadasa, H. I.; McGehee, M. D. Reversible photo-induced trap formation in mixed-halide hybrid perovskites for photovoltaics. *Chem. Sci.* **2015**, *6*, 613−617.
(34) Wehrenfennig, C.; Palumbiny, C. M.; Snaith, H. J.; Johnston, M. B.; Schmidt-Mende, L.; Herz, L. M. Fast Charge-Carrier Trapping in TiO2 Nanotubes. *J. Phys. Chem. C* **2015**, *119*, 9159−9168.
(35) Jepsen, P. U.; Schairer, W.; Libon, I. H.; Lemmer, U.; Hecker, N. E.; Birkholz, M.; Lips, K.; Schall, M. Ultrafast carrier trapping in microcrystalline silicon observed in optical pump-terahertz probe measurements. *Appl. Phys. Lett.* **2001**, *79*, 1291−1293.
(36) Bauer, C.; Boschloo, G.; Mukhtar, E.; Hagfeldt, A. Ultrafast relaxation dynamics of charge carriers relaxation in ZnO nanocrystalline thin films. *Chem. Phys. Lett.* **2004**, *387*, 176−181.
(37) Cooke, D. G.; Hegmann, F. A.; Mazur, Y. I.; Wang, Z. M.; Black, W.; Wen, H.; Salamo, G. J.; Mishima, T. D.; Lian, G. D.; Johnson, M. B. Ultrafast carrier capture dynamics in InGaAs/GaAs quantum wires. *J. Appl. Phys.* **2008**, *103*, 023710.
(38) Fekete, L.; Kuzel, P.; Nemec, H.; Kadlec, F.; Dejneka, A.; Stuchlik, J.; Fejfar, A. Ultrafast carrier dynamics in microcrystalline silicon probed by time-resolved terahertz spectroscopy. *Phys. Rev. B: Condens. Matter Mater. Phys.* **2009**, *79*, 115306.
(39) Yin, W. J.; Shi, T. T.; Yan, Y. F. Unique Properties of Halide Perovskites as Possible Origins of the Superior Solar Cell Performance. *Adv. Mater.* **2014**, *26*, 4653.
(40) Schmidt, T.; Lischka, K.; Zulehner, W. Excitation-power dependence of the near-band-edge photoluminescence of semiconductors. *Phys. Rev. B: Condens. Matter Mater. Phys.* **1992**, *45*, 8989.
(41) Shibata, H.; Sakai, M.; Yamada, A.; Matsubara, K.; Sakurai, K.; Tampo, H.; Ishizuka, S.; Kim, K. K.; Niki, S. Excitation-power dependence of free exciton photoluminescence of semiconductors. *Jpn. J. Appl. Phys. Lett.* **2005**, *44*, 6113−6114.
(42) Hamanaka, Y.; Ogawa, T.; Tsuzuki, M.; Ozawa, K.; Kuzuya, T. Luminescence properties of chalcopyrite AgInS 2 nanocrystals: Their origin and related electronic states. *J. Lumin.* **2013**, *133*, 121−124.
(43) Jang, D. M.; Park, K.; Kim, D. H.; Park, J.; Shojaei, F.; Kang, H. S.; Ahn, J. P.; Lee, J. W.; Song, J. K. Reversible Halide Exchange Reaction of Organometal Trihalide Perovskite Colloidal Nanocrystals for Full-Range Band Gap Tuning. *Nano Lett.* **2015**, *15*, 5191−5199.
(44) Nie, W.; Blancon, J. C.; Neukirch, A. J.; Appavoo, K.; Tsai, H.; Chhowalla, M.; Alam, M. A.; Sfeir, M. Y.; Katan, C.; Even, J.; Tretiak, S.; Crochet, J. J.; Cupta, G.; Mohite, A. D. Light-activated photocurrent degradation and self-healing in perovskite solar cells. *Nat. Commun.* **2016**, *7*, 11574.
(45) Verwey, J. Time and intensity dependence of the photolysis of lead halides. *J. Phys. Chem. Solids* **1970**, *31*, 163−168.
(46) Dawood, R.; Forty, A. The electrical conductivity and photo-decomposition of small crystals of lead iodide: part 1. the measurement of electrical conductivity. *Philos. Mag.* **1962**, *7*, 1633−1651.
(47) Yin, W. J.; Shi, T. T.; Yan, Y. F. Unusual defect physics in CH3NH3PbI3 perovskite solar cell absorber. *Appl. Phys. Lett.* **2014**, *104*, 063903.
(48) Iwanaga, M.; Azuma, J.; Shirai, M.; Tanaka, K.; Hayashi, T. Self-trapped electrons and holes in $PbBr_2$ crystals. *Phys. Rev. B: Condens. Matter Mater. Phys.* **2002**, *65*, 214306.

DOI: 10.1021/acsphotonics.7b00797
ACS Photonics 2017, 4, 2813−2820